Mesoscopic conductance fluctuations in $YBa_2Cu_3O_{7-\delta}$ grain boundary junctions at low temperature

A. Tagliacozzo,[1] F. Tafuri,[2,3] E. Gambale,[1,2] B. Jouault,[4] D. Born,[2,3] P. Lucignano,[1,5] D. Stornaiuolo,[1] F. Lombardi,[6] A. Barone,[1] and B. L. Altshuler[7]

[1]*Dipartimento Scienze Fisiche and Coherentia INFM-CNR, Università di Napoli Federico II, Monte S. Angelo via Cintia I-80126, Napoli, Italy*

[2]*Dipartimento di Ingegneria dell'Informazione and Coherentia INFM-CNR, Seconda Università di Napoli, Aversa, I-81031 Caserta, Italy*

[3]*NEST CNR-INFM and Scuola Normale Superiore, I-56126 Pisa, Italy*

[4]*Groupe d'Étude des Semiconducteurs, CNRS, Université Montpellier 2, UMR 5650, cc074, place Eugène Bataillon, 34095 Montpellier Cedex 5, France*

[5]*SISSA, Via Beirut 2-4, 34014 Trieste, Italy*

[6]*Department of Microelectronics and Nanoscience, MINA, Chalmers University of Technology, 41296 Göteborg, Sweden*

[7]*Department of Physics, Columbia University, New York, New York 10027, USA and NEC Laboratories America, Inc., 4 Independence Day, Princeton, New Jersey 08554, USA*

(Received 30 July 2008; revised manuscript received 24 November 2008; published 6 January 2009)

The magnetoconductance in $YBa_2Cu_3O_{7-\delta}$ grain boundary Josephson junctions displays fluctuations at low temperatures of mesoscopic origin. The morphology of the junction suggests that transport occurs in narrow channels across the grain boundary line with a large Thouless energy. Nevertheless the measured fluctuation amplitude decreases quite slowly when increasing the voltage up to values about 20 times the Thouless energy, of the order of the nominal superconducting gap. Our findings show the coexistence of supercurrent and quasiparticle current in the junction conduction even at high nonequilibrium conditions. Model calculations confirm the reduced role of quasiparticle relaxation at temperatures up to 3 K.

DOI: 10.1103/PhysRevB.79.024501 PACS number(s): 85.25.Am, 68.65.−k, 73.23.−b, 74.78.Na

I. INTRODUCTION

In high critical temperature superconductor (HTS) junctions, including grain boundary (GB) structures, it is well established that various interplaying mechanisms contribute to transport with different weights still to be completely defined in a general and consistent framework.[1–3] As in all nonhomogeneous systems, the barrier region will significantly contribute to determine the transport properties across the structure. What is peculiar of HTS is the complicated material science entering in the formation of the physical barrier microstructure. This will depend on the type of device and the fabrication procedure. The material science complexity of HTS may also result in different precipitates and inclusions present at interfaces and grain boundaries, and in some type of inherent lack of uniformity of the barriers.[2] All this has turned into some uncertainty about the nature of the barrier and has originated various hypotheses on the transport properties. The most widespread models are basically all in between two extreme ideas:[2,4–9] on the one hand resonant tunneling through some kind of dielectric barrier;[4–7] on the other, especially in GB junctions, a barrier composed of thick insulating regions separated by conducting channels, which act as shorts or microbridges.[8,9] In most cases the interface can be modeled as an intermediate situation between the two limits mentioned above. A transition from one extreme to the other can therefore take place. What is unfortunately missing is a way to describe this tuning transition through reliable and well-defined barrier parameters (for instance, the barrier transparency). The predominant *d*-wave order parameter symmetry (OPS) is another important factor [1] to which a large part of the phenomenology has been clearly associated.[1–3,10,11] *d*-wave OPS implies the presence of antinodal (high energy) and nodal (low energy) quasiparticles in the conduction across junctions and the absence of sharp gap features in the density of states of the weak link. Recently, low-temperature measurements have proved macroscopic quantum tunneling (MQT) in $YBa_2Cu_3O_{7-\delta}$ (YBCO) GB junctions, stimulating research on coherence and dissipation in such complex systems.[12–14]

In this work we report on an investigation of magnetoconductance at low temperatures for the same type of biepitaxial GB junctions[15] used for the MQT experiments. These structures are very flexible and versatile, guaranteeing, on the one hand, low dissipation[13,14] and, on the other, a reliable way to pass from tunnel-like to diffusive transport on the same chip by changing the interface orientation.[12,15] We give direct evidence of the role played by narrow conduction channels across the GB. These channels may have different sizes and distributions and obviously a different impact on the transport properties. When increasing applied voltage, mesoscopic conductance fluctuations[16–20] appear in our samples at low temperatures, not dissimilar from what is usually observed in normal narrow metal samples.[21] We expect that, in our sample, typical sizes of the current-carrying constrictions L (Ref. 22) range from 50 to 100 nm and, as a consequence, Thouless energy E_c (see Table I) turns out to be quite large when compared to the values usually measured in traditional normal metal artificial systems.[23] The mesoscopic effects persist at voltages about 20 times larger than the Thouless energy. Mesoscopic issues that emerge from the analyses carried out in the present work are tightly connected to the nature of the GB systems: (a) a smooth crossover appears to exist from the coherent conduction mostly driven by the su-

TABLE I. Summary of the results.

Topic	Relative measurement	Extracted parameters	Estimates
Junction geometry	Magnetic pattern: I_C vs H in Fig. 3	$L_x \sim L_y \sim 50$ nm	$E_c \sim 1$ mV
Transport properties	R_N in Fig. 4 and I_cR_N in Fig. 2	$R_N = 400\ \Omega$, $T \gtrsim 257$ mK	$I_cR_N \sim E_c/e$
Mesoscopic fingerprints	Resistance fluctuations in Figs. 5 and 6	$\mathrm{var}[g] \lesssim 1$	
Phase coherence length	Autocorrelation vs ΔH in Fig. 7, PSD in Figs. 8 and 9	$L_\varphi \lesssim 1\ \mu$m	$L_\varphi \sim V^{-1/4}$
Coherent phase breaking time	Autocorrelation vs ΔV in Fig. 10	$\tau_\varphi \sim 400$ ps	$D\tau_\varphi \sim L_\varphi^2$

percurrent, to the magnetoconductance driven by quantum coherent diffusion of quasiparticles across the mesoscopic area when the voltage at the junction increases; (b) in analogy to pairs, quasiparticles also appear to have a large phase coherence as proved by the shape of the power spectrum of the conductance fluctuations up to temperatures of 3 K; (c) the voltage drop appears to be concentrated at the GB, and nonequilibrium does not affect substantially the mesoscopic interference over a wide area of about 1 μm^2.

This work builds upon a previous report where the main ideas have been illustrated.[24] Herein a more complete analysis of the experimental data is carried out. We have applied the "protocol" established in the last 20 years on semiconducting and normal metal nanostructures to our system and we have extracted the characteristic lengths and scaling energies.

In Sec. II we give some details about the sample fabrication. By presenting the magnetic mesoscopic fingerprints of our sample in Sec. III A, we collect evidence of the mesoscopic character of the conductance fluctuations that we have measured. In Sec. III B we derive from the ensemble average of the fluctuations the variance of the conductance, which is presented in Sec. III C.

In Sec. IV we show the conductance autocorrelation for different magnetic fields in an intermediate voltage range. By analyzing the power spectral density we estimate the phase coherence length L_φ, which is found to be $\lesssim L$ at intermediate voltages ($V = 14-18$ mV). The conductance autocorrelation at different voltages allows us to interpret the role of nonequilibrium by defining the voltage dependence of the phase coherence length, as discussed in Sec. V. The discussion of the results can be found in Sec. VI. Our simple model theory well accounts for the experimental results and clarifies the survival of nonlocality in the quantum diffusion in the presence of a large voltage bias. Table I gives additional information on the planning of this work. Our conclusions can be found in Sec. VII.

II. FABRICATION AND AVERAGE TRANSPORT PROPERTIES OF THE SAMPLE

The GB Josephson junctions (JJs) are obtained at the interface between a (103) YBCO film grown on a (110) $SrTiO_3$ substrate and a c-axis film deposited on a (110) CeO_2 seed layer (see Fig. 1). The presence of the CeO_2 produces an additional 45° in-plane rotation of the YBCO axes with respect to the in-plane directions of the substrate.[12] The angle θ of the grain boundary relative to the substrate a and b axes is defined by suitably patterning lithographically the CeO_2 seed layer [see Fig. 1(a)]. Details about the fabrication process and a wide characterization of superconducting properties can be found elsewhere.[12,15] The interface orientation can be tuned to some appropriate transport regime evaluated through the normal state resistance R_N and critical current density (J_C). Typical values are reported in Fig. 2 and compared with data available in the literature.[3]

In the tilt cases $J_C \approx 10^3$ A/cm^2 and $\sigma_N = 1/(R_NA) \approx 0.2$ (mΩ cm^2)$^{-1}$, both measured at $T = 4.2$ K (where A is the junction cross section). Twist GB junctions are typically characterized by higher nominal values of J_C in the range of $(0.1-4.0) \times 10^5$ A/cm^2 and $\sigma_N \approx 10$ (mΩ cm^2)$^{-1}$ (at $T = 4.2$ K).

We have selected YBCO grain boundary junctions and measured their I-V curves at low temperatures T as a function of the magnetic field H applied in the direction orthogonal to the plane of junction (see Fig. 1(b)). In HTS junctions, the correlation between the magnetic pattern and the current

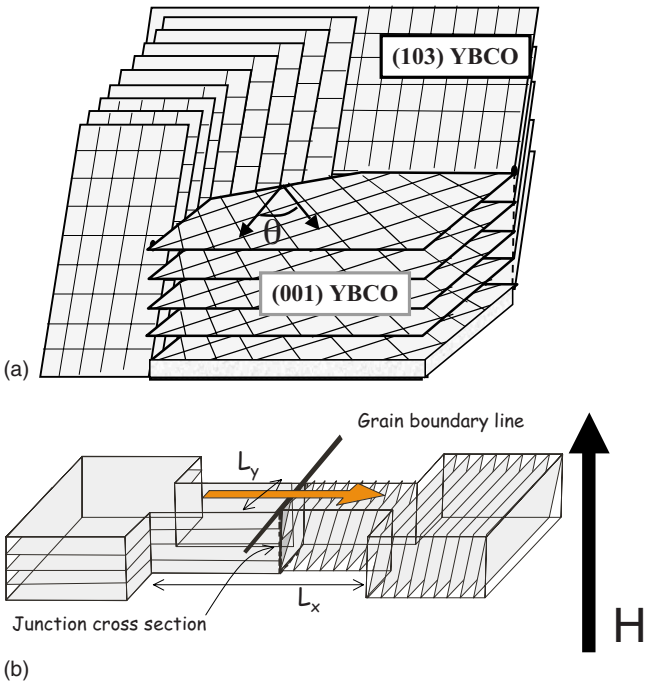

FIG. 1. (Color online) (a) Sketch of the YBCO biepitaxial GB junction used in this experiment. (b) Geometry of the model system of the current-carrying constriction.

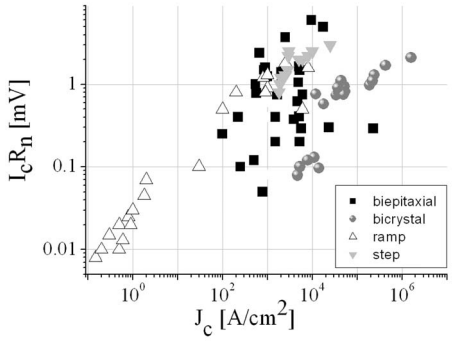

FIG. 2. The product I_cR_N is reported as a function of the critical current density J_c. Data are collected from Refs. 2, 3, and 25–28.

distribution profile along the junction is made more complicated by the *d*-wave OPS, which generates an anomalous magnetic response especially for faceted interfaces.[1–3,29] Additional deviations are expected because of the presence of the second harmonic in the current-phase relation.[10,11] In Fig. 3 we report the magnetic field dependence of the IV characteristic and of the maximum Josephson current of the junction that we have extensively investigated in this work (with barrier orientation θ=60°). This angle gives the maximum J_C.[12] The magnetic response presents a maximum of the critical current at zero field and two almost symmetric lobes for negative and positive magnetic fields, respectively. At higher magnetic fields (above 100 G or below −100 G), the critical current is negligible. The flux periodicity is roughly consistent with the size we expect for our microbridge (50–100 nm) since the London penetration depth in the off-axis electrode is larger than the one in the *c*-axis YBCO films, of the order of microns (see Refs. 14 and 30, for instance). Even if we assume moderate flux-focusing effects, all arguments developed below are only quantitatively slightly affected. Experimental data can be compared with the ideal Fraunhofer case in the crudest approximation without taking into account the presence of a second harmonic or any specific feature of HTS. Even if deviations from the ideal Fraunhofer pattern are present, they can be considered to some extent minor if compared with most of the data on

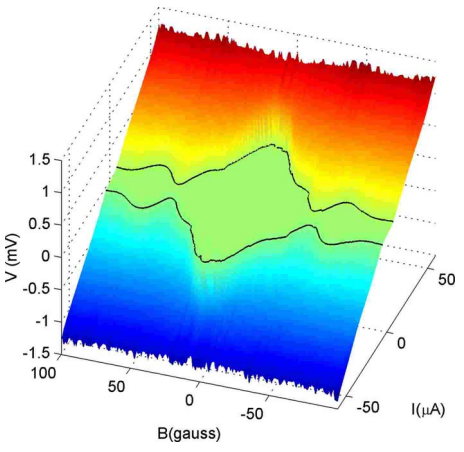

FIG. 3. (Color online) The *I-V* characteristics as a function of magnetic field.

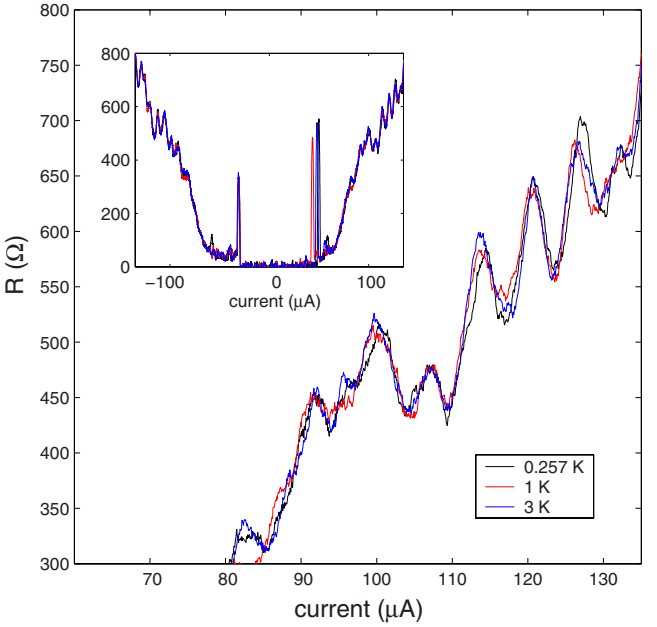

FIG. 4. (Color online) Main: zooming on the oscillations of *R* vs *I* above $I \approx 80$ μA. Inset: Resistance as a function of applied bias current for three different temperatures: 257 mK, 1 K, and 3 K.

HTS grain boundary Josephson junctions, which present radical differences.[2,3] We can infer a uniformity of the junction properties approximately on an average scale of 20–30 nm, which is remarkable if compared with most results available in the literature. Even if we cannot draw any conclusion on the current distribution on lower length scales[31] we can rule out the presence of impurities of large size along the width of the active microbridge. In fact, if there were more than one active microbridge, the current of each of them would add in parallel and the pattern would present other periodicities referring to the area enclosed between the conduction channels.[31] The *I-V* characteristics of the HTS Josephson junctions still present features which cannot be completely understood in terms of the classical approaches used to describe the low critical temperature superconductor Josephson junctions. These are frequently observed and often referred to in the literature as unconventional features.[1–3] Examples are as follows.[3] (a) I_CR_N values are much lower than the gap value Δ. (b) The shape of the *I-V* strongly depends on the critical current density. (c) *I-V* curves show significant deviations from the resistively shunted junction (RSJ) model. (d) There is a poor consistency between the amplitude of the hysteresis and the extracted values of the capacitance when compared to low-T_C superconductor junctions.

At low temperatures, the resistance vs applied current $R(I)$, as derived from the *I-V* characteristics reported in Fig. 3; is rather temperature insensitive, while the critical current I_C maintains a sizable temperature dependence. In the inset of Fig. 4 we show the resistance $R(I)$ at zero magnetic field for three temperatures: 257 mK, 1 K, and 3 K. $R(I)$ obviously vanishes in the Josephson branch and displays a sharp peak when switching to/from the finite voltage conductance. The data are displayed in order to show the critical current at

$I>0$ and the retrapping current at $I<0$. In Fig. 4 (main panel) we show a blow up of the resistance $R(V)$ in a range of voltage values V between 0.25 and 30 mV at zero magnetic field and for different temperatures $T=257$ mK, 1 K, and 3 K. Measurements have been taken after different cool downs in the time lapse of 2 years to study the sample-dependent properties.

The average resistance in the range of voltages $V \approx 10$ mV-15 mV has been stable for about 18 months at $\sim 180\ \Omega$ and has increased in the last year up to about $430\ \Omega$. These changes should be attributed to aging of the diffusion properties at the grain boundary. However, in the meantime, no significant change in the I_C has been detected. Only one sample was available with such a reduced width. The steady progress in nanotechnology will probably lead to the realization of reliable microbridges of nominal width of a few hundred nanometers, from which it will be easier to have junctions with transport carried by very few mesoscopic channels. We finally signal a strong similarity of the I-V and dI/dV-V curves of our junctions with those from submicron YBaCuO junctions reported in Ref. 32.

III. MAGNETORESISTANCE AND MESOSCOPIC FINGERPRINTS

A. Resistance fluctuations

According to what was reported in Sec. II, we figure out that most of the current in the junction substantially flows across a single nanobridge of characteristic size $L_y < 100$ nm. Possible lack of spatial uniformity of the current distribution on a scale of less than 20 nm does not affect the arguments developed below.

We call x the flow direction and y the direction perpendicular to the nanobridge, as shown in Fig. 1(b). The diffusion coefficient D in YBCO is expected to be $\sim 20-24$ cm^2/s.[33] By estimating the Fermi velocity $v_F \approx 7 \times 10^7$ cm/s for optimally doped YBCO, we conclude that the mean free path ℓ is smaller than the size of the nanobridge. Therefore we argue that the transport in the junction is diffusive, which is confirmed by the observation of the resistance fluctuations.

The Thouless energy, as derived from the expected size of the nanoconstriction, is $E_c = \hbar D/L^2 \gtrsim 1$ meV. This value is confirmed by our measurements as discussed in Sec. III. The number of transverse scattering channels in the constriction for a fixed cross section A is approximately $\mathcal{N}_{ch} \approx k_F^2 A \sim 5 \times 10^4$. $A \sim 100 \times 100$ nm^2 is given by the product of the thickness of the film and the width of the channel. Hence, quantization of transverse levels in the bridge does not seem to play any role even at the lowest temperatures investigated. Indeed, $k_B T \gg \delta \sim E_c/\mathcal{N}_{ch} \approx 0.1\ \mu$eV, where δ is the mean energy level spacing. As a consequence, our system can be thought of as a disordered bridge in the diffusive limit $\ell < L$.

We concentrate on the marked nonperiodic fluctuations of the resistance at finite voltages with magnetic field in the range $B=-100-100$ G. An example of the magnetoresistance fluctuations is reported in Fig. 5 (top panel) for $T=257$ mK, 1 K, and 3 K. The fluctuations are not related to the magnetic dependence of the Josephson critical current $I_c(H)$ at voltages $V>2$ mV.

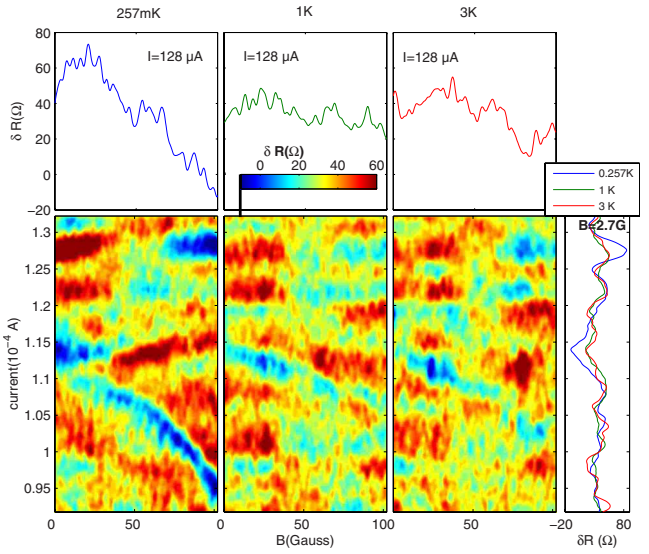

FIG. 5. (Color online) Color plot of the resistance fluctuations $\delta R(H,I)$ as a function of the applied current and of the magnetic field for three temperatures: 257 mK, 1 K, and 3 K. The right panel shows $\delta R(H=2.7G,I)$ vs I for the three different temperatures. The three top panels show single magnetoconductance trace for each temperature at fixed bias current (indicated in the labels).

In order to avoid trapping of flux which may occur when increasing the temperature, especially at the higher fields, the data shown here refer to a single cool down. Occasionally the pattern has still a slight deviation from reproducibility within one single cooling bath, which could be due to finite relaxation in the spin orientation of paramagnetic impurities. The resistance pattern derived from our four terminal measurement does not show any mirror symmetry $R_N(H) \neq R_N(-H)$. Below 1 K there is little temperature dependence. The amplitude of the fluctuations decreases between $T=1$ K and $T=3$ K. They are sample dependent as different cool downs provide different patterns. All these features, as well as the ones described below, strengthen the conclusion that they are mesoscopic fluctuations.

The color plot of the resistance fluctuations in the I,H plane provides the fingerprints of our sample. The deviation from the average $\delta R = R - \bar{R}$ is shown in Fig. 5 (three-color-plot panels) as a color plot for three different temperatures, 257 mK, 1 K, and 3 K. $\bar{R}$ is the average resistance performed over the full range of magnetic fields. The pattern keeps its shape within one single cool down and the contrast of the colors increases in lowering the temperature. The color scale is such that the dark red color refers to resistances significantly larger than the average, while the dark blue color refers to resistances significantly smaller then the average. The data have been filtered by Gaussian convolution to get rid of the underlying white noise.

Despite the small equilibrium thermal length $L_T = \sqrt{\hbar D/k_B T} \sim 0.14\ \mu$m at 1 K, there is a clear persistence of the fingerprints up to $T=3$ K. This suggests that the strong nonequilibrium conditions induced by the applied voltage do

not allow the thermalization of the carriers in the sample. Indeed, our results do not change qualitatively up to 1.5 K, and transport can be classified as nonequilibrium quantum diffusive because $L_\varphi \lesssim L$. Here L_φ is the phase coherence length for carriers diffusing in the junction area and is $\lesssim 1$ μm (see Sec. IV).

B. Ensemble average

The variance var$[g]$ is the ensemble average of the amplitude squared of the conductance fluctuations, $\langle(\delta g)^2\rangle$, where $g=G/(2e^2/h)$ is the dimensionless conductance. We analyze the fluctuations of the conductance obtained by averaging over runs at different magnetic fields up to 100 G at different voltages. Here we argue that this average can be taken as an acceptable ensemble average and provides *bona fide* information about the variance var$[g]$ of the conductance and its autocorrelation. To justify our statement, we have to show that the Cooperon contribution to the variance is not significantly influenced by H up to at least 100 G. The variance of the conductance at equilibrium at temperature T can be calculated as[34]

$$\mathrm{var}[g(H,T)] = \frac{4s^2}{\pi^4}\int \frac{d\Delta E}{2k_BT} f\left[\frac{\Delta E}{2k_BT}\right][F_D(\Delta E,H_1,H_2) + F_C(\Delta E,H_1,H_2)]\Big|_{H_1=H_2=H}, \quad (1)$$

where s is the spin degeneracy, $f(x)=(x\coth x-1)/\sinh^2 x$ and $F_{D,C}$ are the Diffuson and Cooperon autocorrelation functions, respectively. They can be rewritten in terms of the eigenvalues $\lambda_\alpha^{D,C}$ of the diffusion equation,[35]

$$\left\{-D\left[-i\vec{\nabla}+\frac{e}{\hbar c}(\vec{A}_1 \pm \vec{A}_2)\right]^2 + \frac{1}{\tau_{in}} - i\frac{\Delta E}{\hbar}\right\}\psi_\alpha = \frac{\lambda_\alpha^{D,C}}{\tau}\psi_\alpha. \quad (2)$$

Here $D\tau=l^2/d\sim 4\times 10^{-12}$ cm^2 (where d is the effective dimensionality) and τ_{in} is the inelastic relaxation time ($\tau_{in}\gg\tau \sim 0.2$ s). A_1 and A_2 are the vector potentials (H_1 and H_2 are the magnetic fields) influencing the outer and inner conductance loops, respectively, and the $+$ or $-$ sign refers to the C or D propagator, respectively. We have

$$F_{D,C} = L^{-4}(D\tau)^2\sum_\alpha\left[\frac{1}{|\lambda_\alpha^{D,C}|^2}+\frac{1}{2}\,\mathrm{Re}\,\frac{1}{\lambda_\alpha^{D,C^2}}\right]. \quad (3)$$

At zero temperature only $\Delta E=0$ contributes to the integral in Eq. (1) so that the eigenvalues become real. In the evaluation of the variance, $H_1=H_2=H$ implies that the Diffuson eigenvalues become insensitive to the magnetic field. Instead, the Cooperon eigenvalues depend on $2H$ and can be written in analogy with the Landau level energies. It follows that

$$F_C(\Delta E=0,H) \sim \frac{3}{2}\sum_{n=0}^{n_{max}}\frac{1}{\left(n+\frac{1}{2}+\frac{1}{\omega_H\tau_{in}}\right)^2} \sim \frac{3\pi^2}{4}\left(1-\frac{H}{H_0}\right), \quad (4)$$

where $\omega_H=4eHD/\hbar c$. Equation (4) defines a decay threshold field of the Cooperon $H_0\sim \pi hc/(12eD\tau)$, which derives from the truncation of the sum over the orbital quantum number n at $n_{max}\approx\hbar/m\omega_c l^2$ (where $\omega_c=eH/mc$ is the cyclotron frequency). This limitation is required by quantum diffusion ($\langle r^2\rangle_{n_{max}} > l^2$). The large value of n_{max}, in our case ($\sim 10^2$ for $H<600$ G), determines $H_0\gtrsim 2.5$ T which is far beyond the field strengths that can be applied to our sample without trapping flux due to vortices. This confirms that averaging over the interval of H values $H\in(-100-100$ G) is equivalent to a sample average without introducing significant field dependencies. In the following the ensemble average will be denoted by the symbol $\langle\cdots\rangle_H$. As it is shown in Sec. III C, the typical magnetic field scale that arises from the autocorrelation of the conductance is ~ 10 G, much smaller than the interval over which the average is performed.

In the rest of the paper, we will generically denote the conductance autocorrelation, which is an extension of Eq. (1), by K_g. This quantity depends on many variables: T, $H\equiv(H_1+H_2)/2$, $\Delta H\equiv H_1-H_2$, $V\equiv(V_1+V_2)/2$, and $\Delta V\equiv V_1-V_2$. When no ambiguity arises, we have taken the liberty to list just the parameters relevant to the ongoing discussion in order to simplify the notation.

C. Variance of the conductance and different voltage regimes

The conductance is derived from the I/V characteristic. We have checked the behavior of the differential resistance, measured through a standard lock-in method, and we have found qualitatively similar results. In Fig. 6 (upper panel) we have reported the measured conductance fluctuations vs voltage bias and magnetic field at the temperature $T=257$ mK in a gray scale plot. The plot shows two different regimes:

(a) Low voltages ($V<3$ mV) where fluctuations appear to be very high. Fluctuations in this range mostly arise from precursive switching of the current out of the zero voltage Josephson state. The analysis of this range of voltages is better discussed within the macroscopic quantum tunneling dynamics;[13] it requires full account of the superconductive correlations and is not addressed in this paper.

(b) Large voltages ($V>5$ mV). In this regime we observe some reproducible, nonperiodic, and sample-dependent fluctuations. The variance of the conductance $\langle(\delta g)^2\rangle_H$ is plotted vs voltage bias [Fig. 6 (bottom panel)] for two temperatures. The scale for its magnitude is estimated according to $\delta R/R=\delta g/g\approx 0.01$ with $R=410$ Ω($T=300$ mK). The variance var$[g]$ stabilizes around unity at $V\gtrsim 7$ mV. As the voltage increases $V\gtrsim 18$ mV, the variance is increasingly reduced. However, small amplitude fluctuations seem to persist over a wide voltage range up to values which are by far larger than those in normal constrictions. Fluctuations survive up to voltages which are many times the Thouless energy.

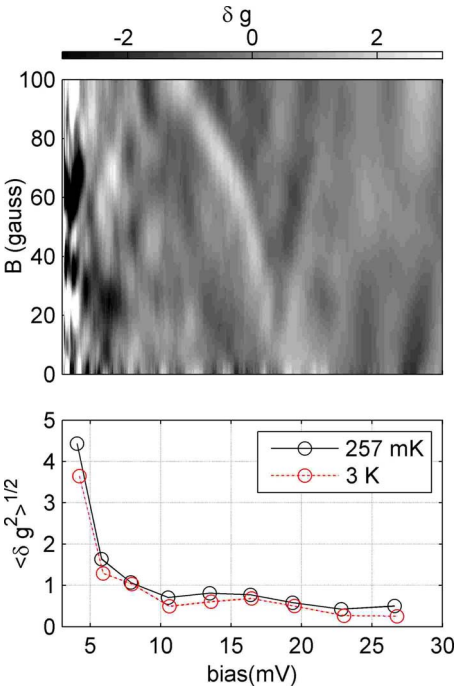

FIG. 6. (Color online) Top panel: gray-color plot of the fluctuations of the dimensionless conductance as a function of the voltage V and of the applied magnetic field H at $T=257$ mK. Bottom panel: Variance of the dimensionless conductance as a function of the voltage V around zero magnetic field for $T=257$ mK and $T=3$ K.

Here we focus on the variance var$[g]$ and on the autocorrelation of the magnetoconductance as a function of voltage at low temperatures up to $V \gg E_c/e \sim 1$ mV. Our data can be interpreted on the basis of models for the quantum interference of carriers transported in the narrow diffusive channel across the GB line. The experimental findings are consistent with a large Thouless energy E_c and quite long dephasing times τ_φ. A comparison of the data with the results of our models seem to confirm that nonequilibrium effects induced by the voltage bias V are not the source of heavy energy relaxation of the carriers, even at voltages $V \gg E_c/e$. A discussion about the voltage dependence of the variance of the conductance for large voltages can be found in Sec. VI. In Sec. IV we analyze the conductance autocorrelation at finite voltage in some detail to extract information about the phase coherence length L_φ and the phase coherence breaking time τ_φ.

IV. SAMPLING NONLOCALITY: AUTOCORRELATION VERSUS ΔH

The variance var$[g]$ of the conductance fluctuations $\langle(\delta g)^2\rangle_H$ discussed in Sec. III C can be derived from the maximum at $\Delta H \approx 0$ of the more general autocorrelation function,

$$K_g(V,\Delta H) \equiv \langle \delta g(V,H+\Delta H)\delta g(V,H)\rangle_H. \qquad (5)$$

The data have been averaged over H, as usual, as well as over a small interval of voltage values about V. K_g is the sum of Cooperon F_C and Diffuson F_D contributions. Due to the

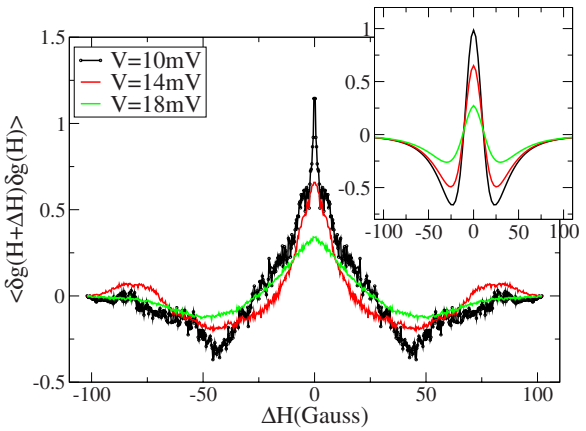

FIG. 7. (Color online) Autocorrelation $\langle(\delta g)^2\rangle$ vs ΔH at $T=257$ mK for three different values of the voltage drop: $V=10$ mV (black curve), $V=14$ mV (red curve), and $V=18$ mV (green curve). Inset: results of the model calculation sketched in the text for $\xi=1.05$ (black curve), 1.15 (red curve), and 1.4 (green curve).

independence of our results of the temperature we consider the zero-temperature limit of Eq. (1). In Fig. 7 we plot the measured autocorrelation of the dimensionless conductance vs ΔH at $T=257$ mK for three values of V: 10 mV (blue curve), 14 mV (red curve), and 18 mV (green curve). The data have been averaged over a voltage interval of width $\delta V=0.5$ mV (the results do not depend on this choice). Similar curves have been measured for normal metal wires at zero voltage bias.[23]

The autocorrelation of Fig. 7 is practically insensitive to increasing temperature up to about 1.5 K. This fact can be viewed as evidence that a significant contribution to transport and to the conductance fluctuations is still provided by the pair current. Its time average and absolute value can be seen as rather temperature and voltage independent at fractions of kelvin, while quasiparticles remain rather frozen, provided that the voltage does not increase too much.[36] For weak links, characterized by higher barrier transparency, the contribution of the supercurrent in the I-V curve can be relevant at finite voltages.[37] The physical reason is that the phase changes in a sharply nonlinear manner with the greater part of the period being close to $\pi/2+2n\pi$. In addition, nonequilibrium effects[38] and unconventional order parameter symmetry (with a not negligible second harmonic component in the current-phase Josephson relation[39]) are possible additional sources of supercurrent flowing at finite voltage. Our results seem to confirm the presence of non-negligible contribution of supercurrent at large voltages from a different perspective. This is consistent with Refs. 37–39 and possibly with the observation of fractional Shapiro steps on YBCO grain boundary Josephson junctions.[40,41]

According to the remark made above, we can assume that the current at $T \sim 0$ is only a function of the phase difference φ between the two superconducting contacts. This assumes little dephasing induced by inelastic scattering processes but not necessarily the absence of quasiparticle contributions to the current which still depends on φ.

The inset of Fig. 7 shows the result of a simple model calculation of the autocorrelation function based on the fol-

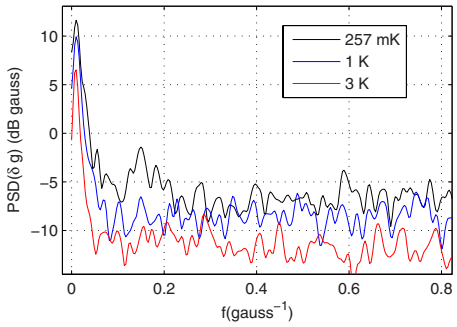

FIG. 8. (Color online) PSD at $T=257$ mK, 1 K, and 3 K and $V=7$ mV averaged over a voltage interval of 0.5 mV. The curves have been shifted for clarity.

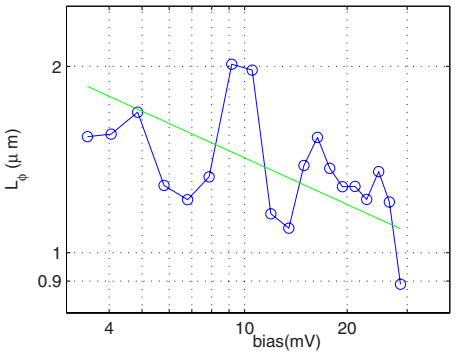

FIG. 9. (Color online) Logarithmic plot of L_φ vs V derived by using Eq. (6). Full lines are a guide to the eye. The slope of the straight line is $-1/4$.

lowing assumptions: (1) negligible proximity effect in the submicron bridge induced by the superconducting contacts; (2) an equilibrium approach to transport, in which the current is mostly phase dependent; and (3) handling of the magnetic field H is treated as a small correction and therefore H only appears in the gauge invariant form of the phase difference.

The model (see Ref. 42 for details) uses a unique fitting parameter $\xi=L_y/L_\varphi$, where L_y is the transverse size of the conduction channel. The curves plotted in the inset are with $\xi=L_y/L_\varphi=1.05$ (black curve), 1.15 (red curve), and 1.4 (green curve). The three different measured curves in the main plot of Fig. 7 refer to different bias voltages and cannot be directly compared to the theoretical curves in the inset of Fig. 7. The qualitative agreement between experimental and theoretical curves is evident, provided we assume that ξ increases with increasing voltage. This assumption is feasible since, on the one hand, L_φ is likely to be reduced when increasing applied voltage, and the number of conduction channels increases by changing the voltage and, as a consequence, the effective width of the bridge. If we assume that L_φ scales with voltage as $V^{-1/4}$ (see discussion in Sec. V), we find that ξ's, which have been chosen to draw the inset of Fig. 7, are consistent with the voltages of the experimental curves within 15% of error.

The qualitative fit, based on the simple theoretical model used here, gives evidence of the fact that nonequilibrium does not seem to spoil the autocorrelation as a function of the magnetic field even if the voltage bias exceeds the Thouless energy: $eV>E_c$. While the dephasing time τ_φ is discussed in Sec. V here we are in a position to extract the value of the phase coherence length L_φ from the power spectral density (PSD) of the conductance autocorrelation function.

The PSD of the conductance autocorrelation is plotted in Fig. 8 vs f_H, the conjugate variable to the magnetic field ΔH, for data at $T=273$ mK, 1 K, and 3 K and $V=7$ mV. f_H has the dimension of an inverse magnetic field. Inspection of Fig. 8 shows that there is a linear slope at small frequencies and a roughly flat trend at larger frequencies. The latter is due to the white noise affecting the measurement. Curves have been shifted, in the figure, for clarity. In reality, both the linear slope and the constant value are almost independent of the temperature. The linear slope allows us to extract the value of the phase coherence length L_φ according to the fit,[43]

$$\log[\mathrm{PSD}/\mathrm{PSD}(f_H=0)]=-2\pi f_H H_c+\mathrm{const}, \tag{6}$$

and correlation field H_c can be related to L_φ as follows: $L_\varphi \sim \sqrt{hc/2eH_c}$. From this plot we derive $H_c\sim 10$ G which gives $L_\varphi \lesssim 1$ μm. A logarithmic plot of the V dependence of $L_\varphi(V)$ is reported in Fig. 9. The straight line drawn among the experimental points shows the functional dependence $V^{-1/4}$.

V. NONEQUILIBRIUM EFFECTS ON τ_φ

In this section we study the dependence of the autocorrelation function on V and ΔV,

$$K_g(V,\Delta V)\equiv\langle \delta g(V+\Delta V,H)\delta g(V,H)\rangle_H. \tag{7}$$

A voltage average has been performed over intervals centered at V of typical size lower than the $\min\{E_c,\Delta V\}$.

In Fig. 10(a) we report the experimental autocorrelation function $K_g(V,\Delta V)$ vs ΔV for various values of the applied voltage V. We stress that the applied voltage is larger than the two natural energy scales: $E_c/e\sim 1$ mV and the nominal superconducting gap $\Delta/e\sim 20$ mV. The tail of the curves

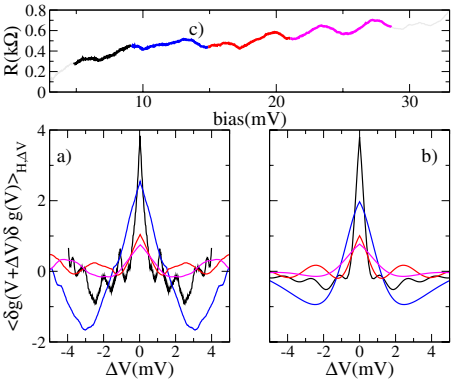

FIG. 10. (Color online) The measured autocorrelation of the conductance $K_g(V,H=0,\Delta V)$ vs the voltage difference ΔV for average voltages $V\approx 7.5$, 12.5, 17.5, and 25.0 mV [panel (a)], theoretical fit based on Eq. (10) [panel (b)], and resistance R vs V [panel (c)]. There is correspondence between the colored ranges of panel (c) and the colors of the curves of panels (a) and (b).

shows a large anticorrelation dip when ΔV increases and damped oscillations. The autocorrelation maximum flattens when the applied voltage V increases. Figure 10(c) emphasizes the voltage range to which each curve of panel (a) refers by using the same color.

We have reproduced the same trend of the data in Fig. 10(a) by assuming that the proximity effect induced by the superconducting contacts does not play an important role in the transport and by adapting the quasi-one-dimensional nonequilibrium theory of Refs. 44 and 45 to our case [see Fig. 10(b)]. We will report on the derivation of our theoretical results elsewhere.[42] We just mention that our nonequilibrium approach gives rise to an autocorrelation $K_g(V,\Delta V)$ which is a function of $x=e\Delta V L^2/\hbar D$ and of the parameters $\tau_\varphi/\tau_{C/D}$ and (L/L_φ).[3] Here $\tau_{C/D}^{-1}=e^2L_y^2D(H_1\pm H_2)^2/(12\hbar^2c^2)$ [with the $+$ $(-)$ sign for the C (D) case] is the relaxation time induced by the magnetic field.[46] In the limit of vanishing ΔV, the result for the variance is recovered, which, up to numerical factors, is given in terms of the ratio between the Airy function $\mathrm{Ai}(u)$ and its derivative with respect to the argument $\mathrm{Ai}'(u)$,

$$K_g(V,\Delta V=0)=-\left(\frac{D\tau_\varphi L_\varphi}{L^3}\right)\sum_{\nu=C,D}\mathrm{Re}\left\{\frac{\mathrm{Ai}\left(\frac{2\tau_\varphi}{\tau_\nu}\right)}{\mathrm{Ai}'\left(\frac{2\tau_\varphi}{\tau_\nu}\right)}\right\}. \quad (8)$$

Here, τ_φ, L_φ, and τ_φ/τ_ν all depend on the voltage. This formula is similar to the thermal equilibrium result by Altshuler-Aronov-Khmielnitski (AAK),[47] which includes the dephasing induced by e-e scattering with small energy transfer. In particular AAK find

$$\frac{1}{\tau_\varphi L_\varphi}=\frac{e^2k_BT}{\hbar^2\sigma}, \quad (9)$$

where σ is the conductivity. At intermediate applied voltages, our zero-temperature prefactor $D\tau_\varphi L_\varphi/L^3$ in Eq. (8) looks similar to the AAK prefactor $\hbar DL_\varphi/(3\pi L^3k_BT)$ if $\hbar/\tau_\varphi$ replaces k_BT.

By choosing an appropriate voltage dependence of the fitting parameter τ_φ/τ_ν and L_φ/L, we find that the autocorrelation scales with $L_\varphi(V)$ as follows:

$$K_g(V,\Delta V)\approx\sum_{\nu=C,D}\mathcal{F}\left[\frac{\Delta V}{V_c},\frac{\tau_\varphi}{\tau_\nu},\left(\frac{L_\varphi}{L}\right)^3\right], \quad (10)$$

with $D\tau_\varphi=L_\varphi^2$, $\tau_C=\tau_D$ and $V_c=\hbar/\tau_\varphi$. The explicit form of the function $\mathcal{F}$ will be given elsewhere.[42] Its limiting form for $\Delta V\to 0$ gives Eq. (8). This scaling law is exploited to plot the curves of Fig. 10(b).

The scaling among the blue, red, and cyan curves reproduces reasonably well the experimental pattern. This indicates that the V dependence of Eq. (10) is well accounted for by simply reducing L_φ with increasing V. On the contrary, the black curve at the lowest voltage $V\sim 7.5$ mV requires adjusting the prefactor after the scaling to make the central peak higher and narrower. This could be a hint to the fact that when the voltage is rather low, the superconducting correlations may be relevant and should be included in deriving the functional form of the $\mathcal{F}$ function. Needless to say, an increase in the τ_φ/τ_ν parameter implies a reduction in the value of $\mathrm{var}[g]$. In writing Eq. (10), extra contributions arising from the nonlinear response have been neglected. Actually, Eq. (10) would be the result within linear response theory only, except for the V dependence of $L_\varphi(V)$.

The global interpretation of the data given here shows that a monotonous decrease in τ_φ with increasing voltage is not achieved. A nonmonotonous decrease in $\mathrm{var}[g]$ vs V is indeed found, as can be seen from Fig. 6. According to the correspondence $D\tau_\varphi=L_\varphi^2$ and to Fig. 9, a general decreasing trend of $K_g(V,\Delta V)$ with increasing voltage could take over only above 20 mV. In Eq. (8) derived from our model calculation, we have found $\hbar/\tau_\varphi$ in place of k_BT appearing in the AAK result of Eq. (9). At larger voltages the expected substitution in Eq. (9) is[45] $k_BT\to eVL_\varphi/L$ and, by requiring the consistency,

$$\frac{L_\varphi}{L}\sim\sqrt{D\tau_\varphi|_{eVL_\varphi/L}}\to\left(\frac{L_\varphi}{L}\right)^4=\frac{D}{L^2}\frac{\hbar g}{eV}, \quad (11)$$

where $g=\hbar\sigma/(e^2L)$ in $1-d$. This would give a decay law for the coherence length $L_\varphi\sim V^{-1/4}$, which is not clearly recognizable in our experiment.

VI. DISCUSSION

We recollect here the main experimental facts that can be extracted from the data, on the topic of quantum transport in a GB YBCO JJ. The magnetic dependence of the maximum critical current suggests an active transport channel of the order of 50–100 nm. Uniformity of the critical current is on scales larger than about 20 nm. The Thouless energy $E_c=\hbar D/L^2$ turns out to be the relevant energy scale in this case. The normal resistance R_N of the HTS junction is of the order of 200 Ω, increasing up to 480 Ω with time due to aging of the sample. The zero-field Josephson critical current appears to satisfy $I_cR_N\sim E_c/e$. This product is definitely much smaller than Δ/e, where the nominal superconducting gap is $\Delta=20$ meV. This represents additional evidence that the proximity effect induced in the bridge in the absence of applied voltage is of mesoscopic origin. The superconductive pair coherence length $\xi_s<L_\varphi\lesssim L$, as opposed to the classical regime, $L<\xi_s$, when the tail of the order parameter enters both superconductors of the junction.[48] We speculate that the oscillations in the resistance as a function of V, shown in the inset of Fig. 4, could be due to this mesoscopic origin.

Remarkable conductance fluctuations have been found in a voltage range up to $20E_c$ in the magnetic field range of $H\in(-100,100)$ G for temperatures below 3 K. In the explored window, we do not measure a halving of the variance with increasing field H.[49] The crossover field H_0 at which the Cooperon contribution to the variance is expected to disappear, as given by Eq. (4), is estimated of the order of few teslas.[49] Decoherence induced by the Zeeman energy splitting requires even larger fields.

Transport has been measured in highly nonequilibrium conditions. Hence the temperature dependence is quite weak up to $T\sim 1.5$ K. We have concentrated our analysis in the voltage range $V\in(7,30)$ mV where the conductance fluctua-

tions reach a steady value for the variance at T below 1 K, $\mathrm{var}[g](V) \lesssim 1$. These properties confirm that the fluctuations are due to quantum coherence at a mesoscopic scale.

The PSD of the autocorrelation of the conductance at different fields ΔH allows us to identify $H_c \approx 10$ G as the field scale for the mesoscopic correlations, weakly dependent on V. This value leads to a phase coherent length $L_\varphi \lesssim 1$ μm. We have plotted the coherence length extracted from the autocorrelation PSD vs V in Fig. 9 and compared it with $L_\varphi(V) \sim (V/V_0)^{-s}$ with $s \sim 0.25$.[45] A similar exponent has been found in a limited range of voltage bias $V > E_c/e$ in gold samples,[50] in which universal conductance fluctuation and Aharonov-Bohm oscillations were found. Dephasing mechanisms are low-frequency electron-electron interaction, magnetic impurity-mediated interaction,[51] and nonequilibrium quasiparticle distribution.[52] According to Fig. 9, the comparison is not conclusive. As a matter of fact, all data of conductance autocorrelation at finite voltage reported for normal wires[23,50] identify a Thouless energy $E_c \sim 1$ μeV, 3 orders of magnitude smaller than in our HTS device, and refer to applied voltages not larger than mV's. Still, mesoscopic coherence persists in our sample up to voltages much larger than the Thouless energy. We do not find any linear increase in the conductance autocorrelation with voltage at large voltages.[44]

Our model calculation appears to reproduce the gross features in the dependence of the conductance autocorrelation $K_g(V, \Delta H, \Delta V)$ on ΔH as well as on ΔV. In the case of $K_g(V, \Delta H, 0)$ we limit ourselves to the linear response term only and the effect of the voltage bias just appeared as a small reduction of $L_\varphi(V)$ with increasing V.

To model the trend of $K_g(V, 0, \Delta V)$ vs ΔV given by the experiment, nonequilibrium cannot be ignored. Our derivation extends the calculation of Refs. 44 and 45. We give a simple estimate of the conductance autocorrelation to fit our experiments. We invoke the simplest nonequilibrium distribution for diffusing quasiparticles, that is, the collisionless limit,[52] by lumping the relaxation processes in the damping parameter of the Cooperon/Diffuson propagators $\tau_{C/D}$. The dependence on the applied voltage is introduced by tuning τ_φ. We obtain oscillations in the negative tail of the autocorrelation, $K_g(V, 0, \Delta V)$ (see Fig. 10) and our scaling procedure fulfills the relation $D\tau_\varphi = L_\varphi^2$. Extra contributions that are specific of the nonequilibrium theory and are known to be responsible first for a linear increase in the autocorrelation function with V and subsequently for its power-law decay are not included here.

VII. CONCLUSIONS

We have reported about transport measurements of high-quality biepitaxial grain boundary YBCO Josephson junction at temperatures below 1 K performed over a time period of about 18 months. A global view on the data offers a consistent picture, pointing to transport across a single superconducting-normal-superconducting-like diffusive conduction channel of mesoscopic size $L \lesssim 0.1$ μm. We have mostly explored the magnetoconductance fluctuations in the voltage range $eV \gg E_c \gg k_B T$, where the Thouless energy $E_c \sim 1$ meV. The Thouless energy 2–3 orders of magnitude larger than the one usually experienced in normal mesoscopic or low-T_c superconducting samples, determines qualitatively the quantum coherent diffusion in the channel. We believe that the oscillations in the resistance that can be seen in Fig. 4 can be due to quantum diffusion.

The mesoscopic correlations are found to be quite robust in our GB narrow channel even at large voltages. This could not occur if the lifetime of the carriers were strongly cut by nonequilibrium relaxation. We conclude that mesoscopic effects deeply involve superconducting electron-electron correlations, which persist at larger voltages. Transport features due to supercurrents and quasiparticles at finite voltages cannot be disentangled in the pattern of the conductance, nor in its variance. This consideration has led us to approach the problem with a nonequilibrium model calculation for generic coherent transport, which highlights the role of the phase breaking time τ_φ without including superconducting correlation explicitly. Figure 10 shows the comparison between our model results and the autocorrelation experimental data, which is encouraging. The remarkably long lifetime of the carriers, which we find, appears to be a generic property in high-T_c YBCO junctions as proved by optical measurements[33] and macroscopic quantum tunneling.[13]

ACKNOWLEDGMENTS

Enlightening discussions with I. Aleiner, H. Bouchiat, V. Falko, A. Golubov, Y. Nazarov, H. Pothier, A. Stern, and A. Varlamov at various stages of this work are gratefully acknowledged. This work has been partially supported by MIUR PRIN 2006 under the project "Macroscopic Quantum Systems—Fundamental Aspects and Applications of Non-conventional Josephson Structures," EC STREP project MIDAS "Macroscopic Interference Devices for Atomic and Solid State Physics: Quantum Control of Supercurrents," and CNR-INFM within ESF Eurocores Programme FoNE-Spintra (Contract No. ERAS-CT-2003-980409).

[1] C. Tsuei and J. Kirtley, Rev. Mod. Phys. **72**, 969 (2000).
[2] H. Hilgenkamp and J. Mannhart, Rev. Mod. Phys. **74**, 485 (2002).
[3] F. Tafuri and J. R. Kirtley, Rep. Prog. Phys. **68**, 2573 (2005).
[4] R. Gross, L. Alff, A. Beck, O. Froehlich, D. Koelle, and A. Marx, IEEE Trans. Appl. Supercond. **7**, 2929 (1997).
[5] R. Gross and B. Mayer, Physica C **180**, 235 (1991).
[6] J. Halbritter, Phys. Rev. B **48**, 9735 (1993).
[7] J. Halbritter, Supercond. Sci. Technol. **16**, R47 (2003).
[8] B. H. Moeckly, D. K. Lathrop, and R. A. Buhrman, Phys. Rev. B **47**, 400 (1993).
[9] E. Sarnelli, G. Testa, and E. Esposito, J. Supercond. **7**, 387 (1994).
[10] T. Löfwander, V. Shumeiko, and G. Wendin, Supercond. Sci.

Technol. **14**, R53 (2001).
[11] S. Kashiwaya and Y. Tanaka, Rep. Prog. Phys. **63**, 1641 (2000).
[12] F. Lombardi, F. Tafuri, F. Ricci, F. Miletto Granozio, A. Barone, G. Testa, E. Sarnelli, J. R. Kirtley, and C. C. Tsuei, Phys. Rev. Lett. **89**, 207001 (2002).
[13] T. Bauch, T. Lindstrom, F. Tafuri, G. Rotoli, P. Delsing, T. Claeson, and F. Lombardi, Science **57**, 311 (2006).
[14] T. Bauch, F. Lombardi, F. Tafuri, A. Barone, G. Rotoli, P. Delsing, and T. Claeson, Phys. Rev. Lett. **94**, 087003 (2005).
[15] F. Tafuri, F. Miletto Granozio, F. Carillo, A. DiChiara, K. Verbist, and G. Van Tendeloo, Phys. Rev. B **59**, 11523 (1999).
[16] B. L. Altshuler and A. G. Aronov, in *Electron-Electron Interaction in Disordered Systems*, edited by A. L. Efros and M. Pollak (Elsevier, Amsterdam, 1985).
[17] P. A. Lee and T. V. Ramakrishnan, Rev. Mod. Phys. **57**, 287 (1985).
[18] P. A. Lee and A. D. Stone, Phys. Rev. Lett. **55**, 1622 (1985).
[19] P. A. Lee, A. D. Stone, and H. Fukuyama, Phys. Rev. B **35**, 1039 (1987).
[20] B. Al'tshuler and P. Lee, Phys. Today **41**(12), 36 (1988).
[21] F. Pierre, A. B. Gougam, A. Anthore, H. Pothier, D. Esteve, and N. O. Birge, Phys. Rev. B **68**, 085413 (2003).
[22] L_x and L_y mark the lengths of the conducting bridge at the junction parallel and perpendicular to the current flow respectively (see Fig. 1) when a distinction is required.
[23] A. van Oudenaarden, M. H. Devoret, E. H. Visscher, Y. V. Nazarov, and J. E. Mooij, Phys. Rev. Lett. **78**, 3539 (1997).
[24] A. Tagliacozzo, D. Born, D. Stornaiuolo, E. Gambale, D. Dalena, F. Lombardi, A. Barone, B. L. Altshuler, and F. Tafuri, Phys. Rev. B **75**, 012507 (2007).
[25] D. Dimos, P. Chaudhari, and J. Mannhart, Phys. Rev. B **41**, 4038 (1990).
[26] H. Hilgenkamp and J. Mannhart, Appl. Phys. Lett. **73**, 265 (1998).
[27] Z. G. Ivanov, P. Å Nilsson, D. Winkler, J. A. Alarco, T. Claeson, E. A. Stepantsov, and A. Y. Tzalenchuk, Appl. Phys. Lett. **59**, 3030 (1991).
[28] K. Char, M. Colclough, S. M. Garrison, N. Newman, and G. Zaharchuk, Appl. Phys. Lett. **59**, 733 (1991).
[29] J. Mannhart, H. Hilgenkamp, B. Mayer, Ch. Gerber, J. R. Kirtley, K. A. Moler, and M. Sigrist, Phys. Rev. Lett. **77**, 2782 (1996).
[30] F. Tafuri and J. R. Kirtley, Phys. Rev. B **62**, 13934 (2000).
[31] A. Barone and G. Paternò, *Physics and Applications of the Josephson Effect* (Wiley, New York, 1982).
[32] F. Herbstritt, T. Kemen, L. Alff, A. Marx, and R. Gross, Appl. Phys. Lett. **78**, 955 (2001).
[33] N. Gedik, J. Orenstein, R. Liang, D. A. Bonn, and W. N. Hardy, Science **300**, 1410 (2003).
[34] A. D. Stone, Phys. Rev. B **39**, 10736 (1989).
[35] J. Rammer, *Quantum Transport Theory* (Perseus Book, Reading, MA, 1998).
[36] We are indebited to Helen Bouchiat for this remark.
[37] K. K. Likharev, Rev. Mod. Phys. **51**, 101 (1979).
[38] K. W. Lehnert, J. G. E. Harris, S. J. Allen, and N. Argaman, Superlattices Microstruct. **25**, 839 (1999).
[39] A. A. Golubov, M. Yu. Kupryanov and E. Il'ichev, Rev. Mod. Phys. **76**, 411 (2004).
[40] D. Terpstra, R. P. J. IJsselsteijn, and H. Rogalla, Appl. Phys. Lett. **66**, 2286 (1995).
[41] E. A. Early, A. F. Clark, and K. Char, Appl. Phys. Lett. **62**, 3357 (1993).
[42] A. Tagliacozzo *et al.* (unpublished).
[43] F. Hohls, U. Zeitler, and R. J. Haug, Phys. Rev. B **66**, 073304 (2002).
[44] A. I. Larkin and D. Khmel'nitskii, Pis'ma Zh. Eksp. Teor. Fiz. **91**, 1815 (1986).
[45] T. Ludwig, Ya. M. Blanter, and A. D. Mirlin, Phys. Rev. B **70**, 235315 (2004).
[46] I. L. Aleiner and Ya. M. Blanter, Phys. Rev. B **65**, 115317 (2002).
[47] B. L. Altshuler, A. G. Aronov, and D. E. Khmelnitsky, Solid State Phys. **15**, 7367 (1982).
[48] P. Charlat, H. Courtois, Ph. Gandit, D. Mailly, A. F. Volkov, and B. Pannetier, Czech. J. Phys. **46**, 3107 (1996).
[49] J. S. Moon, N. O. Birge, and B. Golding, Phys. Rev. B **56**, 15124 (1997).
[50] C. Terrier, D. Babić, C. Strunk, T. Nussbaumer, and C. Schönenberger, Europhys. Lett. **59**, 437 (2002).
[51] A. Kaminski and L. I. Glazman, Phys. Rev. Lett. **86**, 2400 (2001).
[52] H. Pothier, S. Guéron, N. O. Birge, D. Esteve, and M. H. Devoret, Phys. Rev. Lett. **79**, 3490 (1997).